Accepted Manuscript

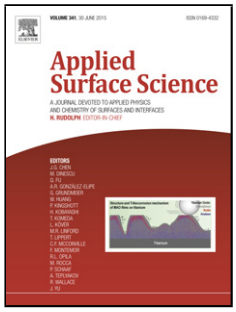

Title: Electrodeposition of Gold Templated by Patterned Thiol Monolayers

Author: Zhe She Andrea DiFalco Georg Hähner Manfred Buck

PII: S0169-4332(15)03049-4
DOI: http://dx.doi.org/doi:10.1016/j.apsusc.2015.12.054
Reference: APSUSC 32037

To appear in: *APSUSC*

Received date: 12-8-2015
Revised date: 4-12-2015
Accepted date: 5-12-2015

Please cite this article as: Z. She, A. DiFalco, G. Hähner, M. Buck, Electrodeposition of Gold Templated by Patterned Thiol Monolayers, *Applied Surface Science* (2015), http://dx.doi.org/10.1016/j.apsusc.2015.12.054

Electrodeposition of Gold Templated by Patterned Thiol Monolayers

Z. She, A. DiFalco, G. Hähner, M. Buck

Highlights

- First demonstration of electrodeposition/lift-off of gold using thiol monolayers
- Microelectrode structures with large length to width ratio were generated
- Performance of two different patterning techniques was investigated
- Conditions for achieving good contrast in the electrodeposition were established

Graphical Abstract (for review)

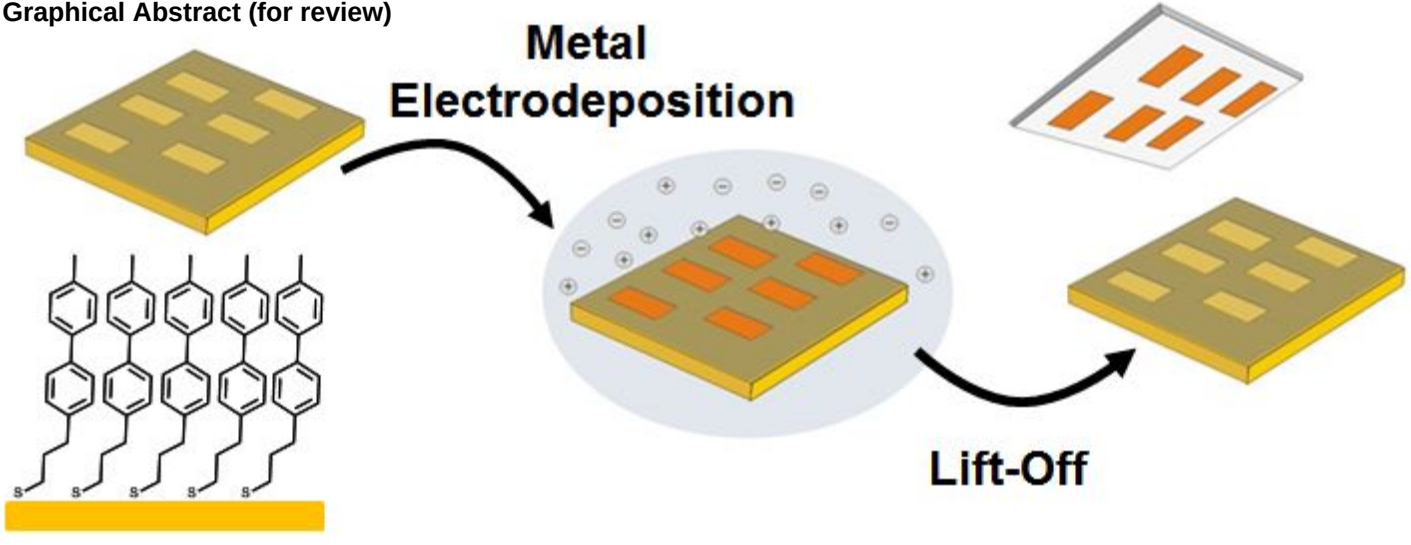

Electrodeposition of Gold Templated by Patterned Thiol Monolayers

Zhe She[1†], Andrea DiFalco[2], Georg Hähner[1], Manfred Buck[1*]

[1]EaStCHEM School of Chemistry, University of St. Andrews, KY16 9ST, U.K.

[2]School of Physics and Astronomy, University of St. Andrews, KY16 9ST, U.K.

[†]present address: Department of Physical and Environmental Sciences, University of Toronto Scarborough, 1265 Military Trail, Toronto, ON, M1C 1A4, Canada.

Email:

* Corresponding author: mb45@st-andrews.ac.uk

Abstract

The electrochemical deposition of Au onto Au substrates modified by self-assembled monolayers (SAMs) was studied by linear sweep voltammetry (LSV), atomic force microscopy (AFM) and scanning electron microscopy (SEM). Patterned SAMs exhibiting electrochemical contrast were prepared by two different methods. One used microcontact printing (μCP) to generate a binary SAM of ω-(4'-methyl-biphenyl-4-yl)-propane thiol (CH_3-C_6H_4-C_6H_4-$(CH_2)_3$-SH, MBP3) and octadecane thiol ($CH_3(CH_2)_{17}SH$, ODT). Templated by the SAM, a gold microelectrode structure was electrodeposited featuring a line 15 μm wide and 3 mm long. After transfer to an epoxy substrate the structure proved to be electrically conductive across the full length. The other patterning method applied electron beam lithography (EBL) where electrochemical contrast was achieved by crosslinking molecules in a single component SAM of MBP3. An electron dose above 250 mC/cm^2 results in a high deposition contrast. The choice of parameters for the deposition/lift-off process is found to be more critical for Au compared to Cu studied previously. The origin of the differences and implications for nanoscale patterning are discussed.

Keywords

metal deposition; nanotechnology; electrochemistry; thiols; lithography; self-assembled monolayers

1. Introduction

The optical and electrical properties of metallic micro- and nanostructures are of interest for a wide range of applications which comprise plasmonics and metamaterials [1-4], energy conversion [5], displays [6], and sensing [7-13]. Besides their technical specification, one important criterion influencing their technological implementation is the effort required to generate such structures and in search for viable routes a widely adopted strategy is based on templating. One variant of this approach is the use of masks such as colloidal layers [10] which are single-use but easy to fabricate by exploiting self-assembly. The self-assembly process allows the generation of the metal structure directly on the substrate of choice, although it limits the templating to periodic patterns and imposes constraints with respect to the accessible geometries and dimensions. Freely definable patterns are accessible using templates which are generated by conventional lithography. However, the effort required to generate them represents a bottleneck and might even become prohibitive for the routine generation of small scaled structures. A solution to this dilemma is the templated deposition using a reusable master pattern followed by a transfer of the structure to another substrate [14-18]. Patterning can either be achieved by a topographic pattern [16, 19] or by a selective deposition onto a flat substrate. The latter is exploited in a scheme where a self-assembled monolayer (SAM) controls the electrodeposition of metal as illustrated in Fig. 1 [17, 20]. An electrode is modified by a patterned SAM which defines electrochemically active and passive areas (1) in the sense that the onset of deposition is at a more negative potential in the passive compared to the active areas as indicated by schematic linear sweep voltammograms (LSV) in Fig. 1. Selective deposition (2) is achieved by setting the deposition potential E_D to a value which is between the onsets of the deposition in the active and passive areas. As illustrated by the cartoon showing a cross-section of a deposit in an active area, there are point contacts between the deposited metal and the substrate. They are located at defects in the SAM at which the deposition starts. After the initial stage where the metal nucleates at the substrate it grows beyond the SAM in a mushroom like fashion until a closed layer is formed. The decisive point is that the area of direct contact between the deposited metal and the substrate metal is very small compared to the area between the deposited metal and the SAM. Since the adhesion energy associated with the metal-organic interface is low the structure can be lifted off by breaking the necks of the deposit [21]. This is accomplished by attaching another substrate (3) which adheres well to the metal deposit but poorly to the blocking SAM. Using

mechanical force the secondary substrate with the pattern is separated from the master electrode (4) which might then be reused (5).

Since the contrast between blocking and non-blocking areas is determined by differences in the defects, selective deposition can be accomplished in two ways. One strategy is based on a binary SAM of thiols where the pattern is defined by two different types of molecules which differ in their ability to block electrodeposition such as a long chain aliphatic thiol (blocking) and a shorter aromatic thiol (non-blocking) [20]. The other one uses chemical modification of a single component SAM for which strategies are available. One option is the fragmentation of a SAM molecule which can be done in a well defined way by e.g. photolytic cleavage [22] or less selectively by electrons [23] to alter the thickness and/or structure of the SAM and, thus, its ability to block electrodeposition. A complementary possibility exploiting the opposite effect is the electron induced crosslinking of molecules which occurs in aromatic SAMs [24-26]. The crosslinking eliminates defects or at least reduces them in size to the extent that a sufficient electrochemical contrast compared to the non-irradiated areas is established [17, 27-29]. Notably, employing this negative resist behaviour of aromatic molecules offers the advantage that the deposition occurs on the native layer, i.e., deposition behaviour and adhesion are defined by the intact SAM molecules. This contrasts thiols comprising aliphatic chains which exhibit positive resist behaviour [23, 30] by undergoing fragmentation, thus, making the control of properties more difficult. For larger scale patterns the binary SAM seems a good choice as patterns can be easily generated by microcontact printing (μCP) [31]. Crosslinking molecules in a single component SAM is the choice for the nanoscale as the high resolution of electron beam lithography can be harnessed [17, 32].

So far defect mediated metal electrodeposition on SAM modified electrodes has mostly been applied to Cu [17, 20-23, 27-30, 33-43] whereas other metals such as Au [44-48], Ag [40, 49-54], Ru [55], Ni [35, 56], Co [27, 57] or a magnetic CoNiFe alloy [14] have been studied more sporadically. Even narrower is the range of metals for the combination of electrodeposition with the lift-off and transfer where with the exception of the CoNiFe alloy [14] only Cu has been studied [17, 20, 21]. While Cu is of interest for its electrical properties, other metals such as Au and Ag are preferred for optical applications. As part of our efforts to widen the knowledge base and the scope of the deposition/lift-off scheme we studied the Au deposition on both binary SAMs and e-beam patterned SAMs. From evaporation experiments it is well known that the propensity to penetrate SAM depends on the type of metal as well as

the structure and terminal group of the SAM [58-60]. Therefore, it was of interest to see to what extent differences between metals exist.

Applying μCP the generation of electrodes with one dimension in the micrometer range and a large length to width ratio was studied which was motivated by a simple access to inert microelectrodes suitable for electroanalysis [61]. In this case the challenge was the uniform deposition over millimeter distances to yield conducting wires. The experiments using e-beam lithography is motivated by its high spatial resolution and, thus, its possibility to generate Au nanostructures.

The type of thiols used in this study has been successfully applied to the deposition of Cu and Co in the past [20, 27-29]. For the binary SAM, octadecane thiol ($CH_3(CH_2)_{17}SH$, ODT) and 3-(4'-methylbiphenyl-4-yl)-propane-1-thiol (CH_3-C_6H_4-C_6H_4-$(CH_2)_3SH$, MBP3) served to define electrochemically passive and active areas. MBP3 is a representative of a class of thiols which combine a short aliphatic chain with an aromatic moiety, a molecular architecture which has been shown to yield high quality monolayers [62, 63]. Furthermore, the aromatic moiety accounts for a negative resist behaviour upon irradation with low energy electrons [29, 64], thus, making it suitable for high resolution patterning.

2. Experimental

2.1 Fabrication of PDMS stamp

The PDMS stamp used for making the two component SAM by μCP was fabricated by moulding a silicon/SU8 master pattern. A silicon chip was cleaned with acetone for 5 mins followed by immersion in isopropyl alcohol for 5 mins in an ultrasonic bath. The chip was ashed in oxygen plasma to remove impurities and improve polymer adhesion. An SU8 layer was coated by spin-coating at 5000 rpm for 1 min with solution prepared by mixing SU8 2050.0 (Microchem) and SU8 2000.5 (Microchem) with a volume ratio of 1:1. The coated chip was baked at 333 K for 1 min and 373 K for 4 mins. The pattern consisting of two rectangular areas (350×450 μm^2) connected by a line (3000×15 μm^2) was written by electron beam lithography (hybride RAITH Elphy Plus/LEO 1530 lithography) at 30 kV and an electron dose of 15 $\mu C/cm^2$. The chip was baked for 2 mins at 373 K after exposure, developed in ethyl lactate for 1 min and baked overnight at 468 K.

The PDMS stamp was prepared by placing the Si/SU8 template in a petri dish and adding a 1:8 mixture of curing agent/silicone elastomer (Sylgard 184, Dow Corning) [65]. After

evacuation in a desiccator for 3 hours to remove any bubbles the elastomer was cured at 338 K for 24 hours. After mechanical separation from the silicon/SU8 chip the PDMS stamp was cut to size.

2.2 Preparation of SAM patterns

1 mM ODT (Fluka) and 250 μM MBP3 [66] solutions were prepared by dissolving the respective substances into ethanol (AnalaR Normapur). Substrates (referred to as Au/Si throughout the text) about 1 cm^2 in size were cut from a 100 nm Au/5 nm Ti/Si 4" wafer (Georg Albert PVD).

Uniform SAMs were prepared by immersing a substrate into the ODT or MBP3 solutions, typically over night at either room temperature or 338 K, followed by rinsing with copious amounts of ethanol and drying in a stream of nitrogen.

The ODT/MBP3 SAM pattern was made by immersing the PDMS stamp in the ODT solution for 10 mins and then placing the touch dry stamp onto the substrate for 10 mins by applying a load of 100-110 g. The substrate was then immersed in the MBP3 solution for 2 hours, followed by rinsing/drying.

Single component MBP3 SAMs were patterned by e-beam lithography (RAITH Elphy Plus/LEO 1530) with a 30 kV beam, and exposures varied between 50 and 750 mC/cm^2. To ensure maximal coverage in the non-irradiated areas patterned SAMs were reimmersed in MBP3 solution at room temperature for 8 h and then rinsed/dried as the other samples.

2.3 Electrodeposition and lift-off

The electrochemistry was carried out using a PGSTAT128N potentiostat and NOVA software (Metrohm Autolab) in a home-built electrochemical cell with three-electrode configuration. The SAM modified Au substrates were used as the working electrode (WE) with an area of 40 mm^2. Au wires (Goodfellow, diameter of 0.25 mm) were used as both reference and counter electrodes (RE and CE). A Luggin capillary was used for the Au reference electrode. The electrolyte was made from $HAuCl_4$ (Sigma-Aldrich, 99.999%) in deionised water and adjusted to pH 1 with HCl (Sigma-Aldrich, 37wt. % in water, 99.999%). During the electrochemical deposition the solution was stirred at a speed of 200 to 400 RPM. The voltammetry measurements were done with a step potential of 0.00244 V and a scan rate of 0.01 V/s. After the deposition the substrate was removed from the cell, rinsed with deionised water and dried with nitrogen gas.

The electrochemically deposited metal structures were lifted off from a SAM modified substrate by placing a Teflon plate with a hole onto the sample and filling the hole with epoxy glue (Araldite rapid set). After curing for 24 h at room temperature the epoxy was mechanically separated from the Au/Si substrate.

2.4 Characterisation of the Au structures

The Au structures as deposited and after lift-off were imaged with AFM in contact mode applying a force of 7-13 nN and a scan rate of 0.6-1.2 Hz. For non-conductive AFM Veeco NPS10 silicon nitride tips (nominal spring constants 0.06 N/m and 0.12 N/m) were used. Conductive AFM measurement on the Au/epoxy samples were performed with a doped diamond tip (Veeco DDESP-FM-10, spring constant 2.8 N/m). A force of 400-700 nN was applied at a scan rate of 0.3-1.2 Hz. The tip voltage was set to the minimum value of 1 mV. A Cu wire was attached to one of the pads of Au structure using conductive silver paint (RS). AFM images were analysed using Gwyddion [67] and WSxM software [68].

3. Results

3.1 Electrodeposition on μCP ODT/MBP3 SAMs

To establish the conditions for the gold deposition using the two component SAM template, linear sweep voltammograms of samples uniformly coated with each component were recorded. As seen from Fig. 2 both SAMs significantly shift the onset of the deposition to more cathodic potentials compared to the native Au/Si substrate. MBP3 is the less passivating SAM but the difference in the onset of deposition between the two SAMs is only about 50 mV. A bigger difference like the ~200 mV observed for the Cu deposition on 4'-methylbiphenyl-4-thiol (CH_3-C_6H_4-C_6H_4-SH, MBP0) and hexadecane thiol [17] would make the setting of the deposition parameters and, thus, a good deposition contrast less critical. However, MBP0 is not a viable option here as the Au deposit adhered more strongly to the substrate than Cu, thus, impeding the lift-off process.

For a patterned ODT/MBP3 sample deposition was first carried out at a fixed potential. As exemplified by Fig. 3a which shows the result of a deposition for 10 s at a potential of -0.25 V, a clear boundary is seen between the areas of the respective SAMs with gold preferentially deposited in MBP3 areas. However, the contrast is rather weak and this was also observed at other potentials. Compared to the MBP3 area the density of the deposition is only slightly lower in the ODT areas and the distribution of the deposit appear less

homogeneous with patches of high and low nucleation density coexisting. To improve the contrast we resorted to the deposition involving a potential step where, similar to previous work on Cu deposited on MBP0 [17], a short nucleation phase at rather negative potentials is followed by a growth phase at significantly more positive potentials. With such an approach a pronouncedly improved contrast was obtained as illustrated by Fig. 3b which shows the result of a deposition applying -0.5 V for 0.04 s and -0.15V for 360 s. The deposition is now confined to the MBP3 areas with only a few isolated particles observed in the ODT area.

From the linear sweep voltammograms in Fig. 2 it is seen that the nucleation potential of -0.5 V is well in the region where both SAMs do not represent a significant barrier for Au deposition. Exploiting the difference in the nucleation kinetics between MBP3 and ODT the Au mushrooms grow preferentially in the area of the aromatic SAM at -0.5 V. The mushrooms behaving like bare Au nanoelectrodes further growth can be carried out at a potential of -0.15 V where both native SAMs are blocking (see Fig. 2). We found that the nucleation time is critical and has to be limited to a duration of around 50 ms. Above 100 ms there is a deterioration of the deposition contrast.

With these deposition parameters which yield high contrast between MBP3 and ODT areas, the full deposition/lift-off sequence was run for a test pattern consisting of two pads connected by a line 3 mm long and 15 μm wide. Figure 4 provides a comparison of the metal structure as deposited onto the SAM patterned electrode (Fig. 4a) and after transfer (Fig. 4b), i.e., after steps 2 and 4 of the scheme shown in Fig. 1. Considering the substantial variations in dimension and the large aspect ratio of the line, one important result illustrated by Fig. 4a is that the microcontact printed pattern of MBP3 and ODT is exactly reproduced. Notably, the only defect in the line over the length of 3 mm which is visible under the optical microscope is the one highlighted in the circular close-up. Taking into account that the preparation was not performed in a cleanroom environment and no special cleaning procedure of the μCP stamp was performed it is reasonable to assume that such a defect is caused by a contamination such as a dust grain. The other crucial point is that the fidelity of the transfer process is very good as evidenced by the comparison of Figs. 4a and 4b. Besides the complete transfer of the electrode structure also any defects are transferred like those marked by the red arrows or the defect in the Au line. While the two main criteria for making a working structure, i.e., a continuous uniform deposition and a high accuracy in the lift-off appear to be met, Fig. 4 also pinpoints the necessity for an exact control of the experimental

conditions. Even though the electrolyte was stirred there was still some inhomogeneity in the concentration which is concluded from the observation that in most of the ODT area no Au deposition occurs but, nevertheless in the area framed by the black dotted rectangle in Fig. 4a a substantial deposition is seen. That this arises from concentration gradients and not from variations in the quality of the stamping can be concluded from other samples of uniform SAMs where striae have also been observed. Considering that the nucleation phase is sensitively dependent on the value of the potential applied and its duration it is not surprising that any concentration gradient can also have an adverse effect on the uniformity of the deposition process. The influence of the local electrolyte concentration is also reflected by a difference between the line and the pads since the Au surface exposed after lift-off is slightly rougher in the area of the pad. Also the friction images (not shown), even though the variation in the friction is comparable, show a difference with respect to the graininess in the contrast. On the line it is finer grained than on the pads which indicates that the nucleation and growth depend to some extent on the geometry of the structure. Since the line represents a microelectrode its diffusion field and, thus, the flux of ions is different compared to the one of the pad.

Even though inspection under the optical microscope did not reveal any defects in the Au line (apart from the one discussed) the limited resolution does not allow for the definite conclusion that the line is continuous. However, continuity was proven by electrically contacting the two pads and verifying conduction with a simple Ohmmeter. While the acoustic indicator of the Ohmmeter reliably indicated electrical conduction, the resistivity value was fluctuating over tens of ohms. Since the probes were manually brought in contact with the metal pads which were only 300 nm thick and on a rather soft substrate, this is ascribed to mechanically induced variations in the contact resistance. Therefore, we can only give an upper limit of the resistivity given by the 80 Ω threshold of the acoustic signal which is in the same range as the 16 Ω calculated from the dimensions of the wire (300 nm thickness, 3 mm length, 15 μm width). For a more detailed study one of the pads was electrically contacted using a conductive paint and the line was imaged by conductive probe atomic force microscopy (CP-AFM) at several points along the line at a distance of 1-2 mm from the contacted pad and, thus, conductivity, topography and friction maps were simultaneously obtained. Representative maps and corresponding height profiles are compiled in Fig. 5. In the topography map (Fig. 5a) the 15 μm wide Au line and the areas of

the epoxy on either side are clearly discernible as the boundaries between the wire and the epoxy substrate are characterised by grooves (marked by arrows) which can be tens of nanometers deep. Their origin is not clear at present as several reasons could account for this. It might be a wetting issue, i.e., the epoxy does not advance right to the corner formed by the SAM and the Au line. Another possibility is a shrinking of the epoxy upon curing thus resulting in an adhesive failure in the corner region. Either of the explanations would be a matter of adhesive forces between metal and epoxy. In this context it is worth noting that a formation of grooves has not been observed in analogous experiments using Cu [17, 20] which can be assumed to adhere more strongly to the epoxy than Au due to its ability of coordination bonding and the presence of oxide on the surface able to hydrogen bond.

In the areas of the epoxy substrate point like defects are observed which, highlighted by the dashed and solid circles in Fig. 5, appear either as protrusions or depressions. The majority of these defects are protrusions. From the height profile it is seen that the surfaces of the metal and the epoxy are at the same height which is unsurprising since these are the surfaces facing the flat Au/Si substrate.

An interesting point is the comparison of the topographies of the lift-off structure and the structure as deposited. The height profile (gray line in Fig. 5a, topographic image shown in inset of Fig. 3b) of the latter reveals a substantial roughness of the outer surface in the range of 100 nm for the line with an average thickness of about 300 nm. The corrugation of this surface is determined by the growth conditions and is much higher than the one observed for the transferred structure which is mainly determined by the flatness of the substrate [17]. Since scattering and plasmon excitation are strongly influenced by roughness [69, 70] the difference in the corrugation of the metal surfaces also explains the different optical appearance of the Au structure before and after lift off (Fig. 4). The expected golden colour is seen only after the lift-off whereas the structure as deposited appears red-brown

The structure is also clearly reflected in the friction image which shows a bimodal distribution of values with the metal exhibiting the lower friction compared to the softer epoxy substrate. The defects appearing as protrusion in the topographic image have the same friction as the metal whereas the topographic defects seen as depressions are either not seen at all or only weakly in the friction image. It can, therefore, be concluded that the protrusions consist of localised metal deposits originating from an incomplete passivation of the ODT layer whereas the depressions are dips in the epoxy. The latter can be explained either by

contaminations present on the master electrode which stick too well to the gold substrate to be transferred to the epoxy substrate or by defects in the SAM so pronounced that the deposited gold adhered too well to the substrate. The friction image allowing for a clear identification of the metal and epoxy regions, the sharp boundaries between the two materials contrast the broadened region between the metal line and the epoxy which appears as a groove in the topographic image. Since the sharp boundary in the friction image is located on the metal side of the grooves this lends support to the interpretation given above that the grooves are due to a recessed epoxy glue.

The conduction map (Fig. 5c) is exactly congruent with the friction image with regard to the areas of epoxy and metal. In the area of the Au line the conductivity is so high that the value essentially corresponds to the saturation current. There are some lower current spikes which are interpreted to arise from insulating contaminations on the surface rather than any intrinsic property of the metal deposit. In the epoxy area there is zero conduction which indicates that the point-like metal deposits seen in the topography and friction images are isolated from the metal pattern. Notably, in electroanalytical applications of the metal structure they would not contribute.

3.2 Electrodeposition on electron beam patterned MBP3 SAMs

The high resolution of electron beam lithography and, thus, the possibility to overcome the limitation in the length scale accessible by microcontact printing motivated the extension of the SAM templated gold deposition onto the two component SAM to the one component electron beam patterned MBP3 SAMs. Using a one component SAM the deposition contrast is achieved in this case by rendering the SAM electrochemically passive through crosslinking of the molecules. The effect is demonstrated by the electron micrograph of Fig. 6 which shows an MBP3 SAM with areas exposed to different doses. While the lowest dose of 50 mC/cm^2 gives a poor contrast, it is well developed at 250 mC/cm^2 and does not significantly improve anymore for larger values. The passivation achieved by cross-linking is significantly more effective than passivation by the ODT SAM in the binary SAM which makes the deposition less critical with regard to the choice of the deposition parameters. In contrast to the deposition on the binary ODT/SAM presented in Sec. 3.1 which involved a potential step, a constant potential was sufficient here to achieve high contrast.

The deposition as depicted in Fig. 6 shows a very good contrast for a sufficiently high electron dose. However, the SEM image also highlights that the Au deposit is not continuous which raises the question of how the nucleation and growth can be controlled by the deposition potential. The evolution of the deposition with potential is presented in Fig. 7 which shows results for deposition potentials in the range between -0.35 V and -0.55 V. In the histogram a bimodal distribution is seen. The low height peaks represent the substrate and to allow for direct comparison of the histograms these peaks were aligned to the same height value by applying an offset. It is obvious from the AFM images that the nucleation density increases substantially towards more cathodic potentials with an almost closed layer after a deposition time of 30 s at -0.55 V. Apart from a significant increase in the nucleation density when going to more negative potentials the histogram and the height profile reveal a change in the average height and the distribution of height values. At -0.35 V the distribution is broad and the separation between the maxima of the deposit and the substrate is around 53 nm. This value reduces to 39 nm for -0.45 V and to 29 nm for -0.55 V deposition potential. Therefore, the minimum thickness where a continuous layer is formed and the corrugation of the layer are larger for the deposition at less negative potentials. Firstly, this is the result of a decrease in the nucleation rate due to the strong distance dependence of electron tunneling which requires the metal ions to penetrate deeper into SAM defects. Secondly, once metal mushrooms have grown beyond the outer surface of the SAM they act as Au nanoelectrodes onto which deposition is greatly facilitated compared to the formation of new nuclei at defects in the SAM. The resulting depletion of metal ions close to the interface further increases the barrier for the formation of new nuclei. The difference between growth and nucleation rate gets smaller at more negative potentials which results in smaller deposits at higher density and, thus, thinner layers. However, the defect mediated deposition means that a higher nucleation density also increases the number of links between the substrate metal and the deposited layer. Since this results in a stronger adhesion the optimal deposition potential enabling a lift-off is defined by the compromise between nucleation density and adhesion of the deposit. Consequently a minimum thickness is required to form a continuous gold layer which has to be kept in mind when addressing nanometer dimensions.

Discussion

Compared to studies which only focus on the Au electrodeposition on surfaces uniformly modified by a SAM [44, 47] the step of pattern transfer as essential part of the scheme shown in Fig. 1 requires to consider the deposition process in the context of adhesion of the metal deposit. Furthermore, the patterned deposition introduces the issue of contrast between electrochemically blocking and non-blocking areas. This results in very different requirements for the systems as highlighted by the role of the alkanethiol which serves to suppress metal deposition in the present study, in contrast to a study of how an alkane thiol SAM influences the microstructure of electrodeposited gold [44].

So far the only other metal for which the scheme comprising the SAM templated deposition of patterns and lift-off has been reported is Cu [17, 20]. Comparing both metals the deposition parameters appear to be more critical for Au. This is, firstly, reflected by the fact that deposition at a single potential is sufficient in the case of Cu [20] whereas, in order to limit nucleation to the aromatic SAM, a stepped potential is required in the case of Au with the duration of the nucleation phase in the 50 ms range being essential. Secondly, MBP0 which was successfully applied to deposit Cu on binary [20] and e-beam patterned SAMs [17], failed in the case of Au for the reason that the deposited Au pattern adhered too strongly to the substrate. This issue was addressed by using MBP3 which is not only geometrically longer than MBP0 but also enables a better film quality due to the combination of a short alkane spacer chain with the aromatic moiety [62]. This reduces adhesion due to a lower density of defects where nucleation occurs. However, a consequence of this is a weaker contrast compared to the alkane thiol which was used as the electrochemically passivating component in the binary SAM approach and which was sufficiently passivating in the case of Cu deposition onto the two component SAM where an even shorter chain of 16 carbon atoms was used [20]. The isolated Au grains seen in the ODT regions (Fig. 5) indicate that the electrochemical passivation is not perfect. While this might not be critical in some applications such as electrochemical analysis as they are electrically not connected to the electrode pattern (see Fig. 5c) the contrast could be improved if required by using a thiol with an alkane chain longer than ODT.

Both the more sophisticated deposition protocol and the requirement of an electrochemically more passivating molecule to reduce adhesion of the deposit suggests that the Au species penetrate the SAM more easily compared to Cu. Since different types of and differently sized defects are present in SAMs comprising point like defects, packing defects at domain

boundaries of the SAM and grain boundaries of the polycrystalline substrate, more extended ones arising from impurities and even dynamic ones due to thermal motion of molecules both the nucleation density and the morphology of the deposit are affected by how easily a neutral metal species or a metal ion penetrates at a particular defect. While it is obvious that a higher nucleation density causes an increased adhesion of the metal structure it also affected by the morphology of the mushroom with a thicker neck also increasing adhesion.

Two scenarios of metal penetration at defects can be envisaged. One comprises the reduction of the ion at the SAM-electrolyte interface and subsequent penetration of the reduced metal atom or small clusters formed at the interface at defects in the monolayer. This bears some analogy to metal evaporation onto SAMs where the neutral species impinge on the outer surface of the SAM and then penetrate through to the substrate. Both Au and Cu have been found to penetrate SAMs with chemically inert terminal groups such as CH_3 and no explicit differences in their penetration behaviour has been reported [58, 71, 72].

In the other scenario it is the ionic species which penetrates at defects in the SAM and then gets reduced. This case is considered the dominant one as the electron tunneling from the electrode to the ion involved in the reduction of the metal makes it, to a first approximation, exponentially dependent on the distance of the ion from the electrode. Therefore, the reduction of an ion approaching the surface by penetration at defects is much more likely than at the outer SAM surface. Experimental evidence that the discharge of ions at the outer surface does not seem to play a significant role comes from the fact that under electrochemical deposition conditions where the metal ions do not specifically interact with the end group of the SAM molecules, deposition on top of SAMs has been unsuccessful [73]. Furthermore, if the ions are discharged at the outer surface of the SAM which is accomplished by coordinating the ions to the terminal group of the SAM, the neutral metal species do not penetrate but diffuse at the SAM/electrolyte interface to form 2D islands and 3D clusters on top of the SAM [74-79].

The reason for the difference between Cu and Au can be explained by the difference in the charge of the ions and the rather different redox potentials which are 0.34 V (vs SHE) for the positively charged Cu^{2+}-ion and 1.0 V (vs SHE) for the negatively charged $AuCl_4^-$ complex. In comparison with the potentials of zero charge (PZC) of the SAM coated electrode which are around -0.056 V (vs SHE) for MBPn SAMs [80] and in the range of -0.206 V (vs SHE) for alkane thiols [81] the layer is about neutral or only weakly negatively charged at the

potentials used for the Cu deposition. For the gold deposition the layer is well positive of the PZC which results in an accumulation of the negatively charged Au complex, thus, increasing the propensity for penetration.

The density and size of the nuclei from which the deposition proceeds in a mushroom like growth affects the deposition lift-off scheme as shown in Fig. 1 in different ways with partially opposing effects. On the one hand, it determines the adhesion of the metal pattern to the master substrate. While the total adhesion strength is determined by the contact area of the deposit with both the SAM and the substrate metal, it is the latter which is decisive due to the weak adhesion force exerted by the CH_3 terminated SAMs. To allow transfer of the metal structure, obviously, its adhesion to the secondary substrate must be stronger than to the master template. On the other hand, the density of the nuclei also determines the precision at which contours are defined. The higher the nucleation density the finer grained is the deposit and, thus, the corrugation of contour lines of the deposited pattern. The contour line corrugation of about 10-20 nm realised for Cu/epoxy system [17] seems difficult to achieve for Au/epoxy due the upper limit in the nucleation density for the lift-off. At present the exact origin of the limit is not clear as a weaker adhesion between the Au and the epoxy compared to Cu and/or a larger contact area per defect between the Au deposit and Au of the master substrate can account for the stronger adhesion.

Conclusions and outlook

A scheme comprising the electrodeposition of metal patterns templated by SAMs and lift off onto an insulating substrate has been investigated for Au. Compared to Cu, the only other metal studied so far using the deposition-lift off scheme [17, 20], the deposition parameters turned out to be more critical. For patterned bimolecular SAMs which are straigthforwardly accessible by microcontact printing (μCP) it is the deposition contrast between the two types of molecules which requires a careful choice of the deposition parameters comprising the nucleation time and the potentials of nucleation and growth. The fabrication of a Au microstructure featuring electrical conductivity of a line with dimensions of 15 μm in width and an aspect ratio of 200 is a successful demonstration of the μCP based approach and seen as a decisive step towards the exploitation of the scheme for the facile generation of Au microelectrodes suitable for applications in electroanalytical chemistry.

For e-beam patterned single component SAMs which afford substantially higher spatial resolution compared to μCP, it is found that the decisive factor is not the deposition contrast but two opposing trends related to nucleation. On the one hand, the precision in the contour definition of a deposited pattern depends on the density and spatial distribution of the nucleation centers. On the other hand, the nucleation density and morphology of the deposits determines the adhesion of the deposited metal structure to the substrate and this sets an upper limit in the nucleation density up to which the lift off of the Au is possible. Again, Au is more critical than Cu for which the adhesion problem was not encountered and, thus, it seems unlikely that patterns with features in the 50-100 nm range realised for Cu[17] can be achieved with Au relying on defects present in a native SAM.

The critical role of the nucleation for the deposition/lift off scheme raises the questions what the options are for its control and to what extent this would enable smaller structures. Reiterating that the present and previous work [17, 27-29] has relied on statistically distributed defects in a native SAM the key point is the control of nucleation sites.

One option is to start from defect free SAMs and introduce defects in a controlled way. Using non-crosslinked thiol SAMs, the principle has been demonstrated [50, 82, 83] and recently been applied to the underpotential deposition of Cu producing features down to the sub-20 nm length scale [84]. However, extension to even smaller dimensions and bulk metal deposition should be based on cross-linked SAMs as molecular diffusion in non-crosslinked SAMs has an adverse effect on the resolution. Introducing defects by e.g. focused ion beam would provide a precise way of defining nucleation sites and, furthermore, provide the possibility to adjust the nucleation density to the dimensions envisaged.

A conceptually different option is to actively control the deposition by the SAM molecule instead of relying on defects. The principle has been demonstrated for uniform thiol SAMs featuring tail groups which coordinate metal ions [74-79]. Upon reduction of the ions the metal forms 2D or 3D clusters on top of the SAM. Since the amount and location of the metal deposited is defined by the coordinating SAM molecules this strategy provides an unprecedented precision in the deposition process. With the range of techniques available to pattern SAMs from the micrometer range to the bottom of the nanoscale [32, 85-88] this strategy offers a flexible approach to SAM templated electrodeposition. What remains to be established is the control of the lift-off process since the use of coordinating end groups

instead of inert CH_3 moieties means stronger adhesion between the SAM and the deposit even though for clusters it has been found that they are easily removed [77].

A third option might open up from the recently reported covalent grafting of molecules onto a graphite or graphene surface and subsequent patterning by nanoshaving [89]. Also representing a SAM templating strategy it harnesses the poor adhesion of materials to graphitic surfaces. Provided the grafted layer can be made of a quality that renders the substrate electrochemically passive the deposition will then take place in the areas of the exposed graphite surface. This strategy would extent the previously demonstrated principle of electrodeposition at graphite steps and subsequent transfer [15] to freely definable patterns.

With a number of options existing offering the potential to advance towards the bottom end of the nanoscale it will be interesting to see which strategy turns out to be most promising.

Acknowledgement

The work was supported by EPSRC (EP/E061303/1 and EP/L017008/1). ADF acknowledges support from EPSRC (EP/I004602/1).

References

[1] W.L. Barnes, A. Dereux, T.W. Ebbesen, Surface plasmon subwavelength optics, Nature, 424 (2003) 824-830.

[2] N.C. Lindquist, P. Nagpal, K.M. McPeak, D.J. Norris, S.-H. Oh, Engineering metallic nanostructures for plasmonics and nanophotonics, Rep. Prog. Phys., 75 (2012) 036501.

[3] A. Di Falco, M. Ploschner, T.F. Krauss, Flexible metamaterials at visible wavelengths, New J. Phys., 12 (2010) 113006.

[4] A.C. De Luca, P. Reader-Harris, M. Mazilu, S. Mariggio, D. Corda, A. Di Falco, Reproducible Surface-Enhanced Raman Quantification of Biomarkers in Multicomponent Mixtures, ACS Nano, 8 (2014) 2575-2583.

[5] C.F. Guo, T. Sun, F. Cao, Q. Liu, Z. Ren, Metallic nanostructures for light trapping in energy-harvesting devices, Light-Science & Applications, 3 (2014) e161.

[6] L. Hu, H. Wu, Y. Cui, Metal nanogrids, nanowires, and nanofibers for transparent electrodes, MRS Bull., 36 (2011) 760-765.

[7] R.M. Penner, Chemical Sensing with Nanowires, Annu. Rev. Anal. Chem., 5 (2012) 461-485.

[8] J.J. Gooding, L.M.H. Lai, I.Y. Goon, Nanostructured electrodes with unique properties for biological and other applications, in: R. Alkire, D.M. Kolb, J. Lipkowski, P.N. Ross (Eds.) Advances in Electrochemical Science and Engineering Wiley-VCH, Weinheim, 2009, pp. 1-56

[9] M.E.J. Obien, K. Deligkaris, T. Bullmann, D.J. Bakkum, U. Frey, Revealing Neuronal Function through Microelectrode Array Recordings, Frontiers in Neuroscience, 8 (2015).

[10] M.E. Stewart, C.R. Anderton, L.B. Thompson, J. Maria, S.K. Gray, J.A. Rogers, R.G. Nuzzo, Nanostructured Plasmonic Sensors, Chem. Rev., 108 (2008) 494-521.

[11] A. Tittl, H. Giessen, N. Liu, Plasmonic gas and chemical sensing, Nanophotonics, 3 (2014) 157-180.

[12] B.J. Plowman, S.K. Bhargava, A.P. O'Mullane, Electrochemical fabrication of metallic nanostructured electrodes for electroanalytical applications, Analyst, 136 (2011) 5107-5119.

[13] A. Di Falco, Y. Zhao, A. Alu, Optical metasurfaces with robust angular response on flexible substrates, Appl. Phys. Lett., 99 (2011) 163110.

[14] O. Azzaroni, P.L. Schilardi, R.C. Salvarezza, Templated electrodeposition of patterned soft magnetic films, Appl. Phys. Lett., 80 (2002) 1061-1063.

[15] M.P. Zach, K.H. Ng, R.M. Penner, Molybdenum Nanowires by Electrodeposition, Science, 290 (2000) 2120-2123.

[16] D. Chanda, K. Shigeta, S. Gupta, T. Cain, A. Carlson, A. Mihi, A.J. Baca, G.R. Bogart, P. Braun, J.A. Rogers, Large-area flexible 3D optical negative index metamaterial formed by nanotransfer printing, Nature Nanotechnology, 6 (2011) 402-407.

[17] Z. She, A. DiFalco, G. Hähner, M. Buck, Electron-beam patterned self-assembled monolayers as templates for Cu electrodeposition and lift-off, Beilst. J. Nanotechnol., 3 (2012) 101-113.

[18] O. Azzaroni, M.H. Fonticelli, G. Benitez, P.L. Schilardi, R. Gago, I. Caretti, L. Vazquez, R.C. Salvarezza, Direct nanopatterning of metal surfaces using self-assembled molecular films, Adv. Mater., 16 (2004) 405-409.

[19] O. Azzaroni, P.L. Schilardi, R.C. Salvarezza, Metal electrodeposition on self-assembled monolayers: a versatile tool for pattern transfer on metal thin films, Electrochim. Acta, 48 (2003) 3107-3114.

[20] I. Thom, G. Hähner, M. Buck, Replicative generation of metal microstructures by template-directed electrometallization, Appl. Phys. Lett., 87 (2005).

[21] P.L. Schilardi, O. Azzaroni, R.C. Salvarezza, A novel application of alkanethiol self-assembled monolayers in nanofabrication: Direct molding and replication of patterned conducting masters, Langmuir, 17 (2001) 2748-2752.

[22] P. Prompinit, A.S. Achalkumar, A.S. Walton, R.J. Bushby, C. Walti, S.D. Evans, Reversible metallisation of soft UV patterned substrates, J. Mat. Chem. C, 2 (2014) 5916-5923.

[23] J.A.M. Sondag-Huethorst, H.R.J. Vanhelleputte, L.G.J. Fokkink, Generation of electrochemically deposited metal patterns by means of electron-beam (nano)lithography of self-assembled monolayer resists, Appl. Phys. Lett., 64 (1994) 285-287.

[24] W. Geyer, V. Stadler, W. Eck, M. Zharnikov, A. Gölzhäuser, M. Grunze, Electron-induced crosslinking of aromatic self-assembled monolayers: Negative resists for nanolithography, Appl. Phys. Lett., 75 (1999) 2401-2403.

[25] P. Angelova, H. Vieker, N.-E. Weber, D. Matei, O. Reimer, I. Meier, S. Kurasch, J. Biskupek, D. Lorbach, K. Wunderlich, L. Chen, A. Terfort, M. Klapper, K. Müllen, U. Kaiser, A. Gölzhäuser, A. Turchanin, A Universal Scheme to Convert Aromatic Molecular Monolayers into Functional Carbon Nanomembranes, ACS Nano, 7 (2013) 6489-6497.

[26] A. Turchanin, A. Gölzhäuser, Carbon nanomembranes from self-assembled monolayers: Functional surfaces without bulk, Prog. Surf. Sci., 87 (2012) 108-162.

[27] B. Völkel, G. Kaltenpoth, M. Handrea, M. Sahre, C.T. Nottbohm, A. Küller, A. Paul, W. Kautek, W. Eck, A. Gölzhäuser, Electrodeposition of copper and cobalt nanostructures using self-assembled monolayer templates, Surf. Sci., 597 (2005) 32-41.

[28] G. Kaltenpoth, B. Völkel, C.T. Nottbohm, A. Gölzhäuser, M. Buck, Electrode modification by electron-induced patterning of self- assembled monolayers, J. Vac. Sci. Technol. B, 20 (2002) 2734-2738.

[29] T. Felgenhauer, C. Yan, W. Geyer, H.T. Rong, A. Gölzhäuser, M. Buck, Electrode modification by electron-induced patterning of aromatic self-assembled monolayers, Appl. Phys. Lett., 79 (2001) 3323-3325.

[30] J.A.M. Sondag-Huethorst, L.G.J. Fokkink, Galvanic copper deposition on thiol-modified gold electrodes, Langmuir, 11 (1995) 4823-4831.

[31] J.C. Love, L.A. Estroff, J.K. Kriebel, R.G. Nuzzo, G.M. Whitesides, Self-assembled monolayers of thiolates on metals as a form of nanotechnology, Chem. Rev., 105 (2005) 1103-1169.

[32] A. Gölzhauser, W. Eck, W. Geyer, V. Stadler, T. Weimann, P. Hinze, M. Grunze, Chemical nanolithography with electron beams, Adv. Mater., 13 (2001) 806-809.

[33] S.E. Gilbert, O. Cavalleri, K. Kern, Electrodeposition of Cu nanoparticles on decanethiol-covered Au(111) surfaces: An in situ STM investigation, J. Phys. Chem., 100 (1996) 12123-12130.

[34] H. Hagenstrom, M.A. Schneeweiss, D.M. Kolb, Modification of a Au(111) electrode with ethanethiol. 2. Copper electrodeposition, Langmuir, 15 (1999) 7802-7809.

[35] T.P. Moffat, H. Yang, Patterned Metal Electrodeposition Using an Alkanethiolate Mask, J. Electrochem. Soc., 142 (1995) L220-L222.

[36] M. Nishizawa, T. Sunagawa, H. Yoneyama, Underpotential deposition of copper on gold electrodes through self-assembled monolayers of propanethiol, Langmuir, 13 (1997) 5215-5217.

[37] E.D. Eliadis, R.G. Nuzzo, A.A. Gewirth, R.C. Alkire, Copper deposition in the presence of surface-confined additives, J. Electrochem. Soc., 144 (1997) 96-105.

[38] X.G. Zhang, X.H. Li, H.L. Li, The influence of bromine adsorption on copper electrodeposition on polycrystalline gold electrodes modified with self-assembled monolayers, J. Colloid Interface Sci., 234 (2001) 68-71.

[39] E.D. Eliadis, R.C. Alkire, In situ studies of Cu deposition in the presence of quaternary ammonium salts, J. Electrochem. Soc., 145 (1998) 1218-1226.

[40] N.S. Pesika, A. Radisic, K.J. Stebe, P.C. Searson, Fabrication of complex architectures using electrodeposition into patterned self-assembled monolayers, Nano Letters, 6 (2006) 1023-1026.

[41] M.S. Doescher, J.M. Tour, A.M. Rawlett, M.L. Myrick, Stripping voltammetry of Cu overlayers deposited on self-assembled monolayers: Field emission of electrons through a phenylene ethynylene oligomer, J. Phys. Chem. B, 105 (2001) 105-110.

[42] M. Hepel, E. Tewksbury, Nanogravimetric study of templated copper deposition in ion-channels of self-assembled glutathione films on gold piezoelectrodes, Electrochim. Acta, 49 (2004) 3827-3840.

[43] M. Epple, A.M. Bittner, A. Kuhnke, K. Kern, W.Q. Zheng, A. Tadjeddine, Alkanethiolate reorientation during metal electrodeposition, Langmuir, 18 (2002) 773-784.

[44] G. Pattanaik, W. Shao, N. Swami, G. Zangari, Electrolytic Gold Deposition on Dodecanethiol-Modified Gold Films, Langmuir, 25 (2009) 5031-5038.

[45] J. Wang, G. Duan, Y. Li, G. Liu, Z. Dai, H. Zhang, W. Cai, An Invisible Template Method toward Gold Regular Arrays of Nanoflowers by Electrodeposition, Langmuir, 29 (2013) 3512–3517.

[46] S. Maisch, F. Buckel, F. Effenberger, Preparation of High Quality Electrical Insulator Self-Assembled Monolayers on Gold. Experimental Investigation of the Conduction Mechanism through Organic Thin Films, J. Am. Chem. Soc., 127 (2005) 17315-17322.

[47] Y.C. Yang, S.L. Yau, Y.L. Lee, Electrodeposition of Au monolayer on Pt(111) mediated by self-assembled monolayers, J. Am. Chem. Soc., 128 (2006) 3677-3682.

[48] F. Mirkhalaf, K. Tammeveski, D.J. Schiffrin, Electrochemical reduction of oxygen on nanoparticulate gold electrodeposited on a molecular template, Phys. Chem. Chem. Phys., 11 (2009) 3463-3471.

[49] D. Oyamatsu, M. Nishizawa, S. Kuwabata, H. Yoneyama, Underpotential deposition of silver onto gold substrates covered with self-assembled monolayers of alkanethiols to induce intervention of the silver between the monolayer and the gold substrate, Langmuir, 14 (1998) 3298-3302.

[50] F.P. Zamborini, R.M. Crooks, Nanometer-Scale Patterning of Metals by Electrodeposition from an STM Tip in Air, J. Am. Chem. Soc., 120 (1998) 9700-9701.

[51] N.S. Pesika, F.Q. Fan, P.C. Searson, K.J. Stebe, Site-selective patterning using surfactant-based resists, J. Am. Chem. Soc., 127 (2005) 11960-11962.

[52] T.J. Mullen, P. Zhang, C. Srinivasan, M.W. Horn, P.S. Weiss, Combining electrochemical desorption and metal deposition on patterned self-assembled monolayers, J. Electroanal. Chem., 621 (2008) 229-237.

[53] H. Hagenstrom, M.J. Esplandiu, D.M. Kolb, Functionalized self-assembled alkanethiol monolayers on Au(111) electrodes: 2. Silver electrodeposition, Langmuir, 17 (2001) 839-848.

[54] N.J. Yang, X.X. Wang, Q.J. Wan, Silver nucleation on mercaptoacetic acid covered gold electrodes, Electrochim. Acta, 52 (2007) 4818-4824.

[55] S. Langerock, H. Menard, P. Rowntree, L. Heerman, Electrocrystallization of rhodium clusters on thiolate-covered polycrystalline gold, Langmuir, 21 (2005) 5124-5133.

[56] A. George, A.W. Maijenburg, M.D. Nguyen, M.G. Maas, D.H.A. Blank, J.E. ten Elshof, Nanopatterning of Functional Materials by Gas Phase Pattern Deposition of Self-Assembled Molecular Thin Films in Combination with Electrodeposition, Langmuir, 27 (2011) 12760-12768.

[57] B. O'Brien, K.J. Stebe, P.C. Searson, Octadecanethiol SAMs as molecular resists for electrodeposition of cobalt, J. Phys. Chem. C, 111 (2007) 8686-8691.

[58] G. Nagy, A.V. Walker, Dynamics of the interaction of vapor-deposited copper with alkanethiolate monolayers: Bond insertion, complexation, and penetration pathways, J. Phys. Chem. B, 110 (2006) 12543-12554.

[59] A.V. Walker, T.B. Tighe, O.M. Cabarcos, M.D. Reinard, B.C. Haynie, S. Uppili, N. Winograd, D.L. Allara, The dynamics of noble metal atom penetration through methoxy-terminated alkanethiolate monolayers, J. Am. Chem. Soc., 126 (2004) 3954-3963.

[60] A.V. Walker, T.B. Tighe, J. Stapleton, B.C. Haynie, S. Upilli, D.L. Allara, N. Winograd, Interaction of vapor-deposited Ti and Au with molecular wires, Appl. Phys. Lett., 84 (2004) 4008-4010.

[61] P. Salaun, B. Planer-Friedrich, C.M.G. van den Berg, Inorganic arsenic speciation in water and seawater by anodic stripping voltammetry with a gold microelectrode, Anal. Chim. Acta, 585 (2007) 312-322.

[62] P. Cyganik, M. Buck, J.D.E.T. Wilton-Ely, C. Wöll, Stress in Self-Assembled Monolayers: The Case of ω-Biphenyl-Alkane Thiols on Au(111), J. Phys. Chem. B, 109 (2005) 10902-10908.

[63] W. Azzam, A. Bashir, A. Terfort, T. Strunskus, C. Wöll, Combined STM and FTIR characterization of terphenylalkanethiol monolayers on Au(111): Effect of alkyl chain length and deposition temperature, Langmuir, 22 (2006) 3647-3655.

[64] S. Frey, H.T. Rong, K. Heister, Y.J. Yang, M. Buck, M. Zharnikov, Response of biphenyl-substituted alkanethiol self-assembled monolayers to electron irradiation: Damage suppression and odd-even effects, Langmuir, 18 (2002) 3142-3150.

[65] A. Kumar, G.M. Whitesides, Features of gold having micrometer to centimeter dimensions can be formed through a combination of stamping with an elastomeric stamp and an alkanethiol ‘‘ink’’ followed by chemical etching, Appl. Phys. Lett., 63 (1993) 2002-2004.

[66] H.-T. Rong, S. Frey, Y.-J. Yang, M. Zharnikov, M. Buck, M. Wühn, C. Wöll, G. Helmchen, On the Importance of the Headgroup Substrate Bond in Thiol Monolayers: A Study of Biphenyl-Based Thiols on Gold and Silver, Langmuir, 17 (2001) 1582-1593.

[67] Version 2.37, 2014 http://gwyddion.net/.

[68] I. Horcas, R. Fernandez, J.M. Gomez-Rodriguez, J. Colchero, J. Gomez-Herrero, A.M. Baro, WSXM: A software for scanning probe microscopy and a tool for nanotechnology, Rev. Sci. Instrum., 78 (2007).

[69] H. Kapitza, Influence of surface-roughness on reflection of gold-films in region of surface plasmon excitation, Optics Communications, 16 (1976) 73-75.

[70] M.E. Knotts, K.A. Odonnell, Measurements of light-scattering by a series of conducting surfaces with one-dimensional roughness, J. Opt. Soc. Am. A, 11 (1994) 697-710.

[71] G.C. Herdt, D.R. Jung, A.W. Czanderna, Weak interactions between deposited metal overlayers and organic functional groups of self-assembled monolayers, Prog. Surf. Sci., 50 (1995) 103-129.

[72] Z.H. Zhu, T.A. Daniel, M. Maitani, O.M. Cabarcos, D.L. Allara, N. Winograd, Controlling gold atom penetration through alkanethiolate self-assembled monolayers on Au (111) by adjusting terminal group intermolecular interactions, J. Am. Chem. Soc., 128 (2006) 13710-13719.

[73] H. Haick, D. Cahen, Making contact: Connecting molecules electrically to the macroscopic world, Prog. Surf. Sci., 83 (2008) 217-261.

[74] T. Baunach, V. Ivanova, D.M. Kolb, H.G. Boyen, P. Ziemann, M. Buttner, P. Oelhafen, A new approach to the electrochemical metallization of organic monolayers: Palladium deposition onto a 4,4 '-dithiodipyridine self-assembled monolayer, Adv. Mater., 16 (2004) 2024-2028.

[75] H.G. Boyen, P. Ziemann, U. Wiedwald, V. Ivanova, D.M. Kolb, S. Sakong, A. Gross, A. Romanyuk, M. Buttner, P. Oelhafen, Local density of states effects at the metal-molecule interfaces in amolecular device, Nature Materials, 5 (2006) 394-399.

[76] O. Shekhah, C. Busse, A. Bashir, F. Turcu, X. Yin, P. Cyganik, A. Birkner, W. Schuhmann, C. Woll, Electrochemically deposited Pd islands on an organic surface: the presence of Coulomb blockade in STM I(V) curves at room temperature, Phys. Chem. Chem. Phys., 8 (2006) 3375-3378.

[77] C. Silien, D. Lahaye, M. Caffio, R. Schaub, N.R. Champness, M. Buck, Electrodeposition of Palladium onto a Pyridine-Terminated Self-Assembled Monolayer, Langmuir, 27 (2011) 2567-2574.

[78] M.I. Muglali, J. Liu, A. Bashir, D. Borissov, M. Xu, Y. Wang, C. Woell, M. Rohwerder, On the complexation kinetics for metallization of organic layers: palladium onto a pyridine-terminated araliphatic thiol film, Phys. Chem. Chem. Phys., 14 (2012) 4703-4712.

[79] D. Qu, K. Uosaki, Electrochemical metal deposition on top of an organic monolayer, J. Phys. Chem. B, 110 (2006) 17570-17577.

[80] R. Aguilar-Sanchez, G.J. Su, M. Homberger, U. Simon, T.H. Wandlowski, Structure and electrochemical characterization of 4-Methyl-4'-(n-mercaptoalkyl)biphenyls on Au(111)-(1 x 1), J. Phys. Chem. C, 111 (2007) 17409-17419.

[81] J.A.M. Sondag-Huethorst, L.G.J. Fokkink, Electrical double layers on thiol-modified polycrystalline gold electrodes, J. Electroanal. Chem., 367 (1994) 49-57.

[82] M. Petri, D.M. Kolb, Nanostructuring of a sodium dodecyl sulfate-covered Au(111) electrode, Phys. Chem. Chem. Phys., 4 (2002) 1211-1216.

[83] K. Seo, E. Borguet, Nanolithographic write, read, and erase via reversible nanotemplated nanostructure electrodeposition on alkanethiol-modified Au(111) in an aqueous solution, Langmuir, 22 (2006) 1388-1391.

[84] C. Shen, M. Buck, Nanoscale patterning of a self-assembled monolayer by modification of the molecule–substrate bond, Beilst. J. Nanotechnol., 5 (2014) 258-267.

[85] R.K. Smith, P.A. Lewis, P.S. Weiss, Patterning self-assembled monolayers, Prog. Surf. Sci., 75 (2004) 1-68.

[86] G.J. Leggett, Scanning near-field photolithography-surface photochemistry with nanoscale spatial resolution, Chem. Soc. Rev., 35 (2006) 1150-1161.

[87] M. Liu, N.A. Amro, G.Y. Liu, Nanografting for surface physical chemistry, in: Annu. Rev. Phys. Chem., 2008, pp. 367-386.

[88] C. Shen, M. Buck, Patterning of self-assembled monolayers based on differences in molecular conductance, Nanotechnology, 20 (2009) 245306.

[89] J. Greenwood, T.H. Phan, Y. Fujita, Z. Li, O. Ivasenko, W. Vanderlinden, H. Van Gorp, W. Frederickx, G. Lu, K. Tahara, Y. Tobe, H. Uji-i, S.F.L. Mertens, S. De Feyter, Covalent Modification of Graphene and Graphite Using Diazonium Chemistry: Tunable Grafting and Nanomanipulation, ACS Nano, 9 (2015) 5520-5535.

Figure Captions

Figure 1: Scheme to generate metal structures by SAM templated electrodeposition (1,2), transfer to another substrate (3,4) and reuse of the original template (5). The difference between the electrochemically active and passive areas is illustrated by the LSVs in (1). A model of the metal deposited on the SAM modified electrode is shown in (2). For details see text.

Figure 2: Linear sweep voltammograms of Au deposition from 1 mM $HAuCl_4$ for native (black squares), MBP3 (green triangles) and ODT (red cross) covered Au/Si electrodes. Scan rate 10 mV/s, Au reference electrode. SAMs were prepared at 338 K.

Figure 3: Contrast in the electrodeposition of Au from a 2.6 mM $HAuCl_4$ solution at pH1 onto a Au/Si substrate modified by a binary SAM of MBP3 and ODT. (a) Deposition for 10 s at a fixed potential of -0.25 V. (b) Deposition using a potential step of -0.5 V/0.04 s and -0.15V for 360 s. Large image shows enlarged section of the area marked by the white square on the image shown in the inset. The height profiles are along the white lines indicated. Arrows mark boundary between the SAM areas. Potentials referenced to a Au electrode.

Figure 4. Generation of a Au microelectrode structure by electrodeposition and lift-off. Optical micrographs of the structure as deposited on a Au/Si substrate coated with a ODT/MBP3 SAM pattern (a) and after lift-off using an epoxy resin (b). Red arrows highlight corresponding defects on the structure as deposited and after lift-off. Deposition parameters are the same as in Fig. 3b. Circular close-ups highlight a defect in the Au line. The dotted black rectangle marks a region where deposition has occurred in the area of the ODT SAM as detailed in the text. Due to the high aspect ratio the structure is composed of individual pictures.

Figure 5. Topography (a), friction (b) and current (c) images of the Au line of the microstructure after lift-off as shown in Fig. 4b. For comparison, the gray line in (a) shows the height profile of the Au line before lift-off as shown in the inset of Fig. 3b. Encircled areas in (a) and (b) highlight different types of defects. For details see text.

Figure 6. SEM image of Au electrodeposited on an electron beam patterned MBP3 SAM on Au/Si from a 5 mM $HAuCl_4$ solution for 30 s at -0.35 V. Numbers denote electron dose in units of mC/cm^2. Inset shows enlarged 3×3 μm^2 area marked by the white square. The SAM was prepared at 338K.

Figure 7. AFM images (4×4 μm^2), histograms and height profiles of Au electrodeposited on MBP3/Au/Si from a 5 mM $AuCl_4$ solution for 30 s at -0.35 V (a), -0.45V (b) and -0.55 V (c). Height profiles are along lines shown in the AFM images. The SAM was prepared at 338K.

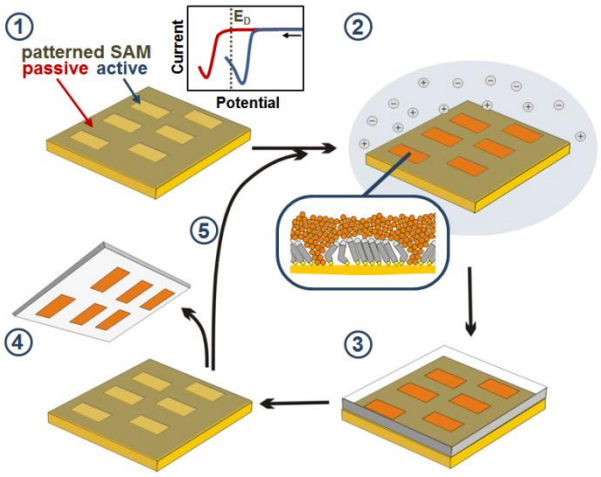

Fig. 1

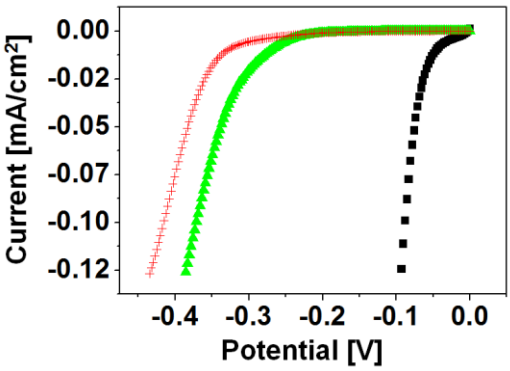

Fig. 2

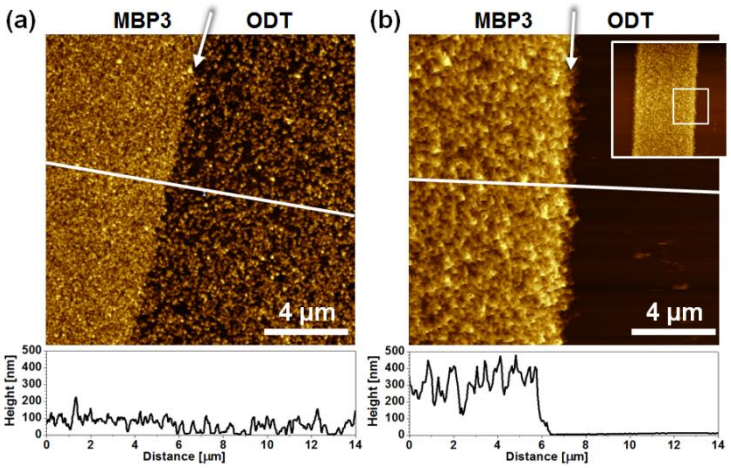

Fig. 3

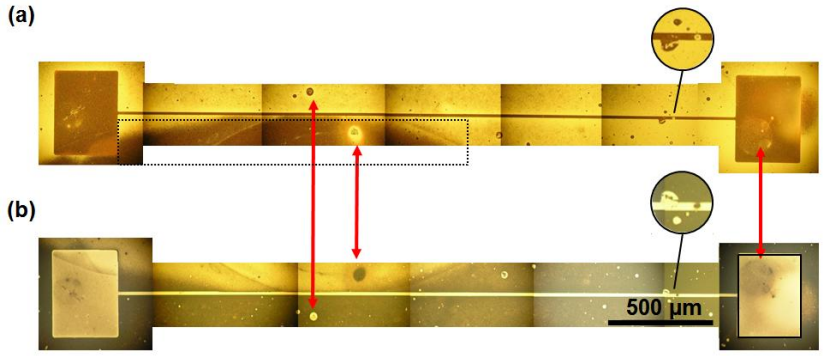

Fig. 4

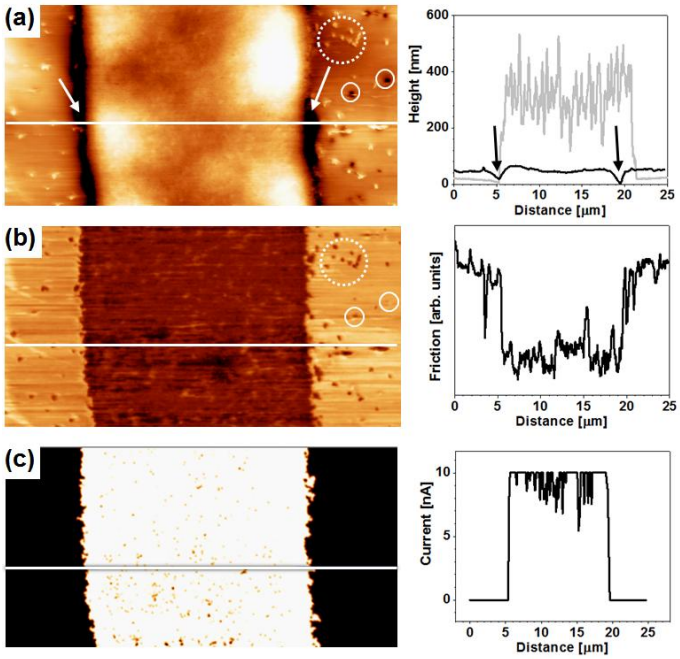

Fig. 5

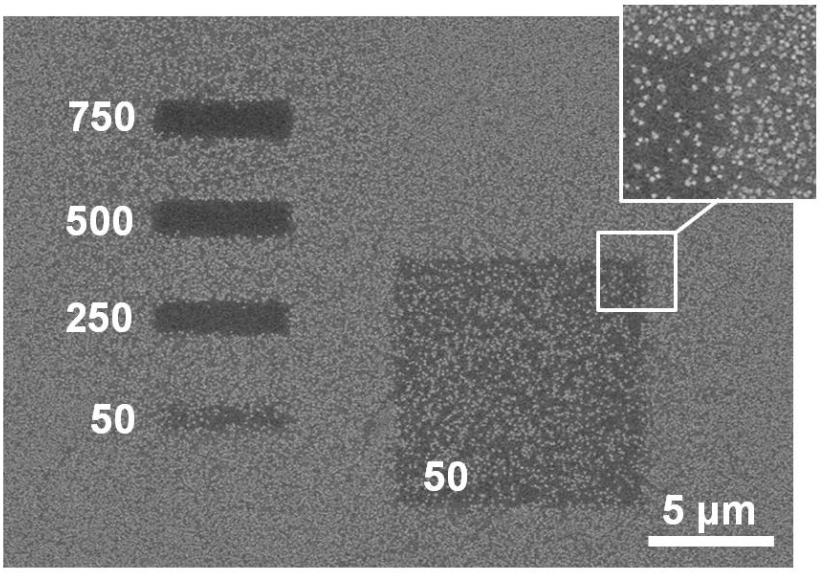

Fig. 6

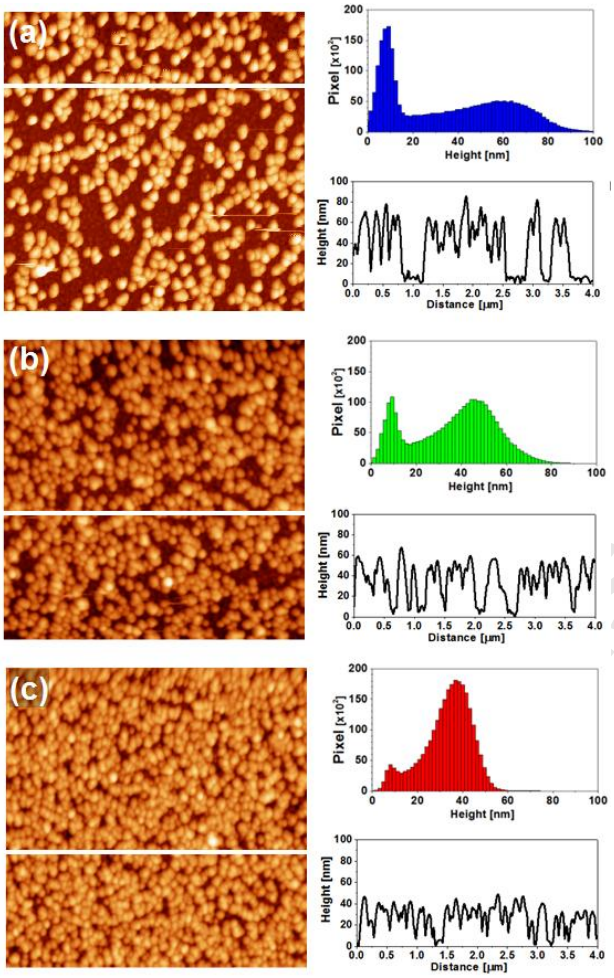

Fig. 7